Supporting Information

Temperature-dependent plasmonic response of graphene nanoresonators

Junhyung Kim[1,†], *Geonwoo Lee*[1,†], *Sergey G. Menabde*[1], *Yong Jai Cho*[2], *Carsten Rockstuhl*[3,4], *Min Seok Jang*[1,*]

[1] School of Electrical Engineering, Korea Advanced Institute of Science and Technology, Daejeon 34141, Republic of Korea

[2] Advanced Instrumentation Institute, Korea Research Institute of Standards and Science, Daejeon 34113, Republic of Korea

[3] Institute of Theoretical Solid State Physics, Karlsruhe Institute of Technology, Wolfgang-Gaede-Str. 1, 76131 Karlsruhe, Germany

[4] Institute of Nanotechnology, Karlsruhe Institute of Technology, P.O. Box 3640, 76021 Karlsruhe, Germany

[†] These authors contributed equally to this work.

[*] E-mail: jang.minseok@kaist.ac.kr

S1 Inhomogeneous linewidth broadening of the GP peak

By analyzing AFM scans of the nanoresonator arrays, we estimate the statistical distribution of the nanoribbons width W: mean value μ_W = 55, 75, 97, and 154 nm, and the standard deviation $\sigma_W \approx 5$ nm. We estimate the broadening of the resonance peaks as follows: (1) Transmission spectra of uniform resonators for normally incident light are calculated using rigorous coupled-wave analysis (RCWA); (2) Assuming the nanoresonator width follows the Gaussian distribution, the transmission spectra of uniform resonators are averaged to take into account resonator inhomogeneity. Due to the variation of resonator widths within the array, resulting extinction peaks tend to have decreased intensity and broader linewidth, as shown in Figure S1 and summarized in Table S1, 2.

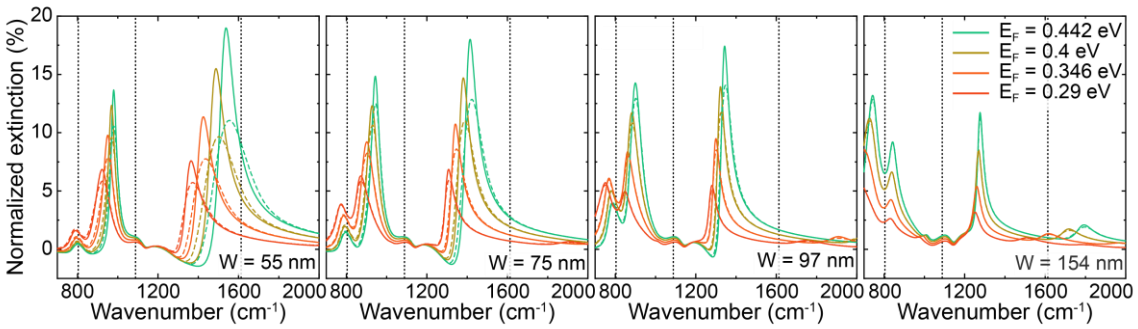

Figure S1. Calculated normalized extinction spectra of graphene nanoresonators on Si/SiO_2 substrate at different Fermi levels in graphene. Solid and dashed curves indicate the normalized extinction spectra of uniform and inhomogeneous resonators, respectively. The inhomogeneous resonators are assumed to have Gaussian width distribution with a standard deviation of 5 nm.

	W = 55 nm	W = 75 nm	W = 97 nm	W = 154 nm
E_F = 0.29 eV	0.771	0.884	0.961	0.997
E_F = 0.346 eV	0.702	0.819	0.910	0.994
E_F = 0.4 eV	0.644	0.770	0.860	0.985
E_F = 0.442 eV	0.604	0.736	0.827	0.973

Table S1. Estimated GP peak intensities of inhomogeneous resonators normalized by those of uniform resonators.

	W = 55 nm	W = 75 nm	W = 97 nm	W = 154 nm
E_F = 0.29 eV	1.472	1.218	1.068	1.004
E_F = 0.346 eV	1.630	1.351	1.160	1.010
E_F = 0.4 eV	1.776	1.454	1.255	1.024
E_F = 0.442 eV	1.877	1.527	1.324	1.043

Table S2. Estimated GP linewidths of inhomogeneous resonators normalized by those of uniform resonators.

S2 Excitation of plasmons in graphene nanoresonators at different temperatures

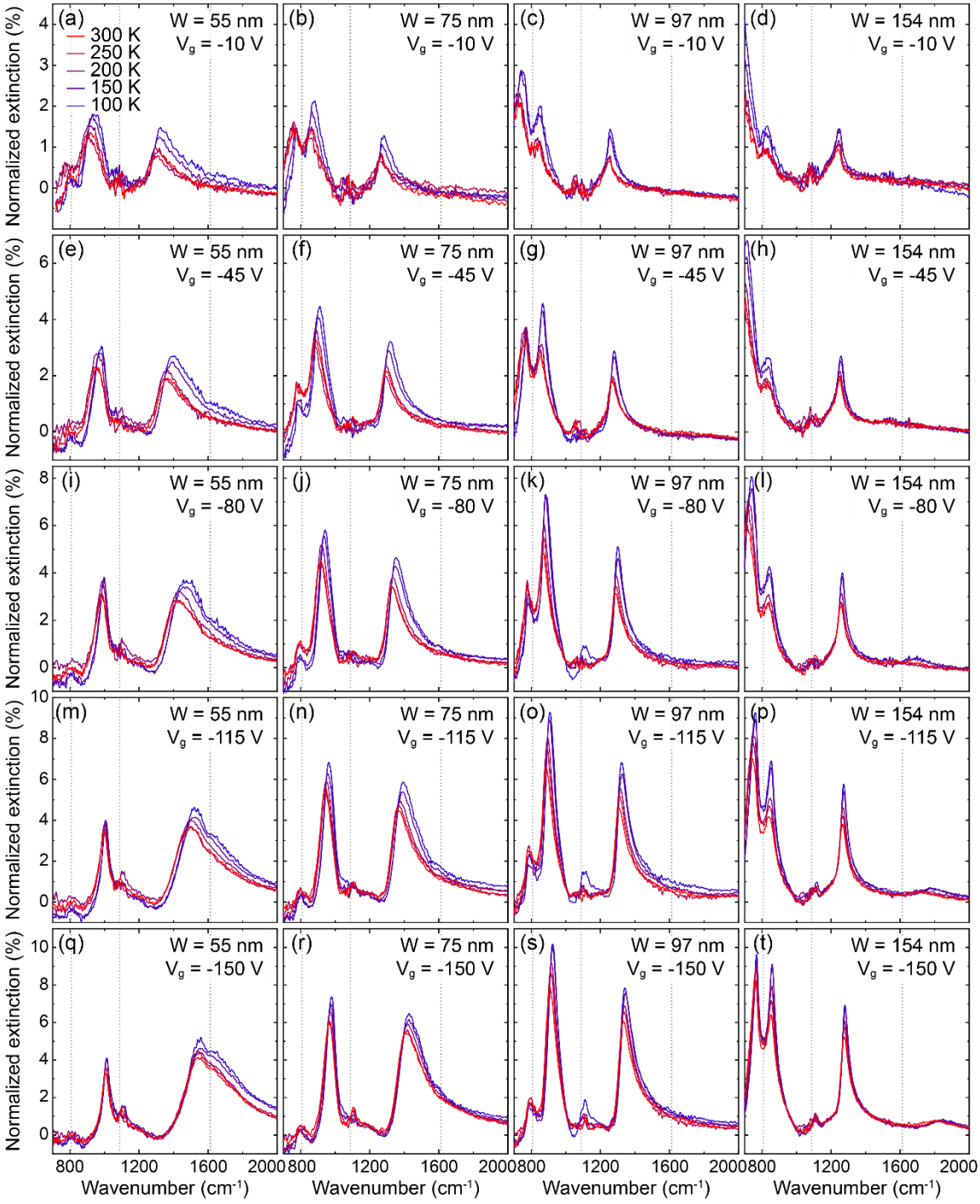

Figure S2. The normalized extinction spectra of various nanoresonator arrays at different temperatures $T \in \{100, 150, 200, 250, 300\}$ K . The resonator width $W \in \{55, 75, 97, 154\}$ nm, and gate bias $V_g \in \{-10, -45, -80, -115, -150\}$ V are specified on the upper right corner of each subfigure.

S3 Mobility extraction using constant mobility model

Figure 2a shows the DC resistance of graphene as a function of the gate voltage at different temperatures. From this, hole mobility can be extracted by using the constant mobility model [Ref 32]. The hole concentrations in the graphene channel region p_{tot} can be calculated as:

$$p_{\mathrm{tot}} = \sqrt{p_0^2 + \left(\epsilon\epsilon_0 \left| V_{\mathrm{CNP}} - V_{\mathrm{g}} \right| / ed\right)^2},$$

where p_0 is the residual hole concentration at the CNP, and the other squared term represents the hole concentration induced by the gate bias. The total device resistance R_{tot} is given by:

$$R_{\mathrm{tot}} = R_{\mathrm{contact}} + R_{\mathrm{channel}} = R_{\mathrm{contact}} + \frac{L/W}{p_{\mathrm{tot}} e \mu}$$

where R_{contact} is the electrode/graphene contact resistance, R_{channel} is the resistance of the graphene channel, and L and W are the length and width of the graphene channel, respectively. By fitting this model to the measured data in Figure 2a, we can extract the mobility value at each temperature. Measured and fitted DC curves are shown in Figure S3, and the extracted temperature-dependent mobility is shown in Figure 2b.

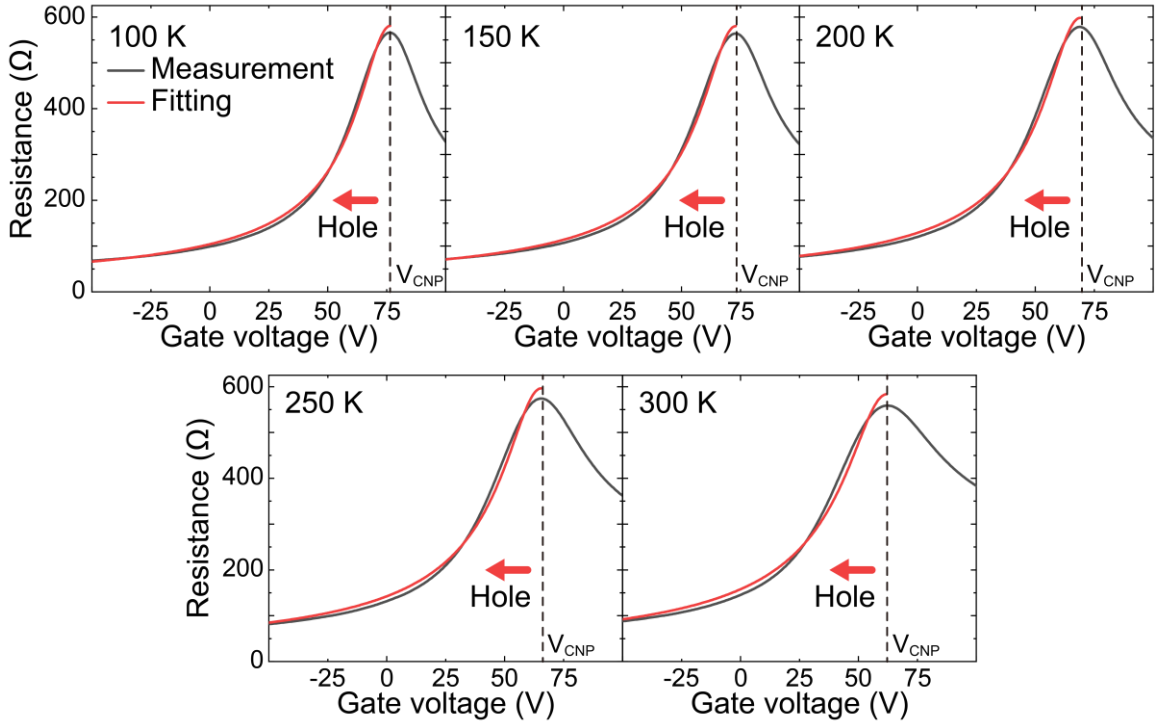

Figure S3. DC resistance of graphene as a function of the gate voltage at different temperatures: measured data (black) and the fit by the constant mobility model (red). Vertical dashed lines indicate the charge neutrality point at each temperature.

S4 Breit-Wigner-Fano(BWF) line shape resonance fitting

Measured FT-IR transmission data were fitted with Breit-Wigner-Fano (BWF) model, which is described as follows[1]:

$$T_{BWF} = \frac{(A/q^2)\left(q\Delta\omega/2 + (\omega - \omega_0)\right)^2}{(\Delta\omega/2)^2 + (\omega - \omega_0)^2}$$

The peak positions were set as the maximum points in the fitted curves, and the peak intensities were obtained by subtracting the baseline from the maximum values.

S5 Carrier concentration fitting by theoretical plasmon dispersion

Doping level variation associated with cooling is estimated through the optically measured extinction peak position of the graphene plasmon. We fit the theoretical dispersion relation of graphene plasmon with the measured extinction peak position, using the doping concentration as the only fitting parameter. When the light is coupled to a graphene plasmon mode having the propagation constant k_{p}, the plasmon experiences reflection at the two edges of the nanoresonator. Hence, when the reflected plasmon waves are in phase, the following constructive interference condition is satisfied:

$$2\mathrm{Re}\{k_{\mathrm{p}}(\omega)\}W + 2\phi = 2m\pi,$$

where W is the width of the nanoresonator, and ϕ is the phase shift of the plasmons upon reflection. We know W from the AFM measurements and estimate ϕ by performing electromagnetic simulations using a finite element method. $k_{\mathrm{p}}(\omega)$ in the non-retarded regime can be approximated as $k_{\mathrm{p}}(\omega) = 2i\epsilon_0\epsilon_{ave}\omega/\sigma(\omega)$. Then, the condition for the first-order (m = 1) plasmon resonance can be reduced to:

$$\frac{\omega_{\mathrm{p}}W}{2\pi}\,\mathrm{Im}\left\{-\frac{\epsilon_{\mathrm{ave}}(\omega_{\mathrm{p}})}{\sigma(\omega_{\mathrm{p}})}\right\} = \pi - \phi$$

where $\epsilon_{\mathrm{ave}}(\omega) = (1 + \epsilon_{\mathrm{SiO_2}}(\omega))/2$, and $\sigma(\omega)$ is the graphene conductivity, which can be calculated within the local random phase approximation[2].

Here, the only unknown parameter is $\sigma(\omega)$, determined by the carrier concentration of graphene. Using the carrier concentration as the only fitting parameter, fitting was performed to minimize the difference between the measured and the theoretical plasmon peak positions calculated from the plasmon resonance condition. The estimated carrier densities are {1.38, 1.13, 0.85, 0.59}×10^{13} cm^{-2} and {1.48, 1.25, 0.99, 0.72}×10^{13} cm^{-2} at T = 300 and 100 K,

respectively, for V_g = -150, -115, -80 and -45 V. Results of this fitting procedure is shown in Figure 4a.

Next, using the previously mentioned equation for the carrier concentration given by:

$$p = Q/e = C\Delta V/e = \epsilon\epsilon_0\left|V_{\mathrm{CNP}} - V_g\right|/ed$$

fitting was performed to minimize the error between the estimated carrier densities and the calculated carrier density using the Dirac voltage V_{CNP} as the only fitting variable. We confirmed that the estimated doping levels well match the linear fit, with a constant doping difference between 300 and 100 K. We associate this doping shift with the additional hole doping due to cooling and estimated its value to be $\Delta p = 1.37 \times 10^{12}$ cm^{-2}. This value is similar to the estimated additional hole doping from the DC electric measurement. These results are shown in Figure 4b.

Moreover, carrier concentration were estimated using the above fitting procedure at each temperature. The estimated cooling-induced carrier concentration (Δp) is shown in Figure S4, demonstrating an abrupt increase of carrier concentration at T < 200K. This trend is consistent with the tendency observed for the GP peak intensity shown in Figure 5.

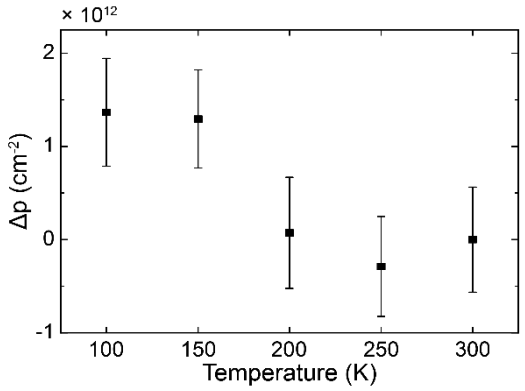

Figure S4. Estimated cooling-induced carrier concentration as a function of temperature obtained from the plasmon dispersion fitting. Error bars indicate the standard deviation of each measured data point.

S6 Si/SiO_2 substrate transmission spectra at various temperatures

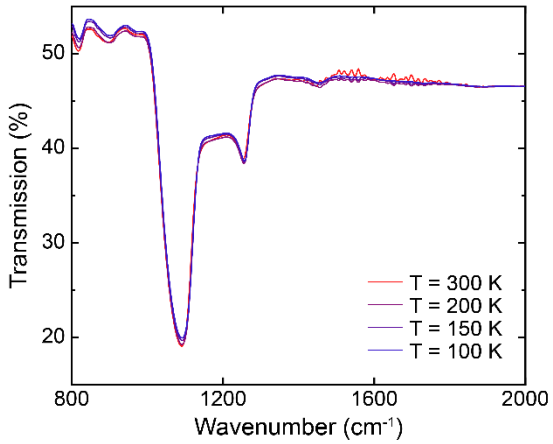

Figure S5. The transmission spectra of bare Si/SiO_2 substrate at various temperatures.

To investigate the temperature dependence of the SiO_2 permittivity, we measured the transmission spectra of a bare Si/SiO_2 substrate at various temperature. As shown in Figure S5, the transmission dip near 1088 cm^{-1} associated with SiO_2 optical phonon gets slightly smaller with decreasing temperature, but the overall transmission spectrum hardly changes with temperature, especially in the frequency range where GP resonances reside. Therefore, we expect the effect of the temperature dependence of SiO_2 permittivity on the graphene plasmon resonance would be marginal.

S7 Optical simulation for fixed GP peak frequency

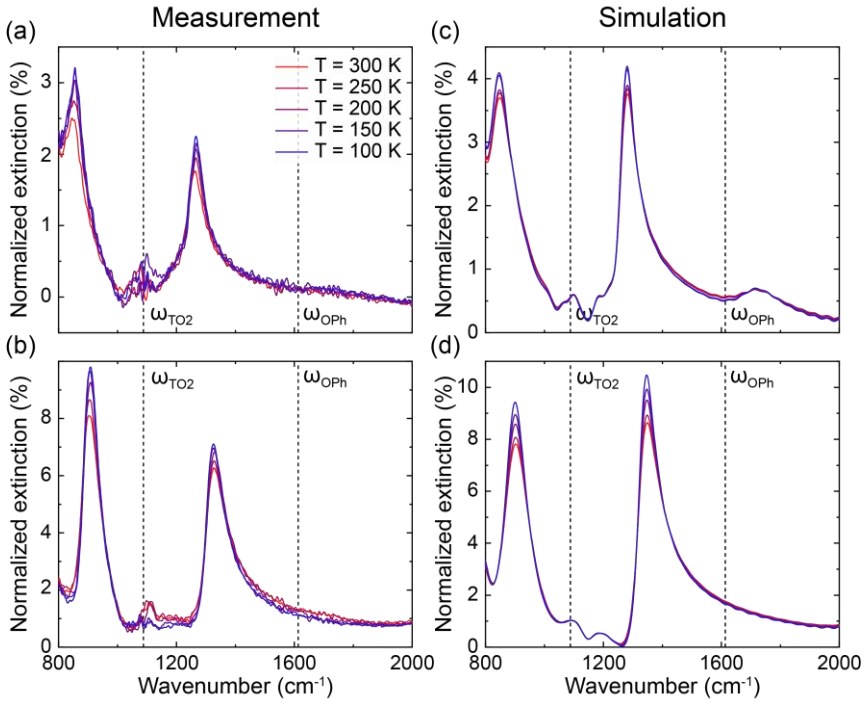

Figure S6. Comparison between the experimental (a,b) and numerically calculated (c,d) extinction spectra of the GP resonance in nanoresonators with W = 97 nm at different temperatures and two values of carrier concentration: (a,c) $p = 1.38 \times 10^{13}$ cm^{-2} and (b,d) 0.59×10^{13} cm^{-2}.

Figures 6a and b show the normalized extinction spectra in a nanoresonator with W = 97 nm at two carrier concentration values $p = 1.38 \times 10^{13}$ cm^{-2} and 0.59×10^{13} cm^{-2} corresponding to GP resonance frequencies of ω_{GP} = 1334 cm^{-1} and 1269 cm^{-1}, respectively. To reproduce these measurement results, we carefully conduct finite-difference time-domain (FDTD) simulations using graphene AC mobility as a variable model parameter. Because of the experimental imperfections such as inhomogeneous width variation and "dead" resonators in the actual device, the measured extinction peaks suffer inevitable intensity decrease and linewidth broadening. Therefore, the AC mobility in the simulations was adjusted based on the linewidth rather than the peak intensity of graphene plasmon resonance. Figures S6c and d show the resulting extinction spectra from the simulations, in good agreement with the measured data. Here, we speculate that the main cause of the discrepancy is the inhomogeneous width variation of the graphene nanoresonators. The simulation shown in Figure S6 were performed under the assumption of constant resonator width. In contrast, in the real system, the resonators are not

perfectly uniform due to the proximity effect during the e-beam lithography. This width variation generally leads to lower peak intensities. However, this effect should be less significant for the SPPP peaks than GP peaks since the SPPP peaks are pinned around the SiO_2 optical phonon line [Ref 9], and thus, their frequency is less sensitive to the resonator inhomogeneity. As a result, the measured GP peaks tend to have a lower relative intensity than the simulated ones (Figure S1).

S8 Comparison between DC and AC hole mobility of graphene

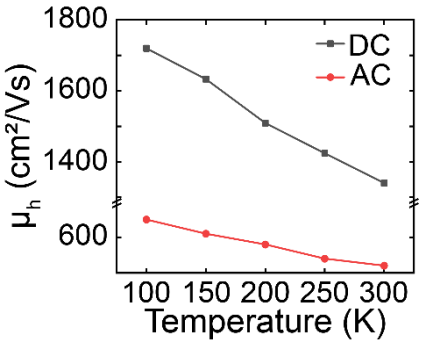

Figure S7. Extracted DC and AC hole mobility of graphene as a function of temperature.

Unlike the DC conductivity, which can be described as a simple product of carrier density and mobility, the optical, i.e., the AC conductivity of graphene is a complicated function of the frequency ω, the Fermi energy E_F, and the temperature T, due to the interplay between interband and intraband electronic transitions. Figure S7 shows the extracted DC and and AC hole mobility of graphene as a function of temperature. As explained above, the DC mobility is extracted by fitting the constant mobility model to the measured DC transport curves. In contrast, the AC mobility is extracted by fitting the linewidth of the GP extinction peak, which reflects a different carrier physics. As a result, the estimated AC mobility is almost three times smaller than its DC counterparts, but the general trend – increasing mobility with decreasing temperature – is preserved. We note that, however, the extraction of AC carrier mobility is not as straightforward and reliable as the DC case because the linewidth of a GP resonance can also be affected by other factors, including the uniformity of the graphene nanoresonators within the measured area and the dispersion and loss of the substrate material.

S9 Temperature dependence of the GP peak frequency

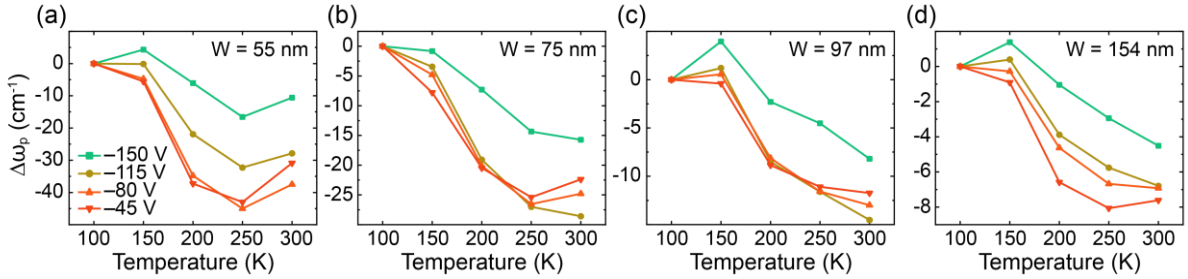

Figure S8. (a)-(d) Temperature dependence of the GP peak frequency shift $\Delta\omega_{\mathrm{p}} = \omega_T - \omega_{100\mathrm{K}}$ for different widths of the nanoresonators W and the gate bias V_{g} specified in the legend in (a).

S10 Width dependence of the normalized intensities of the GP extinction peak

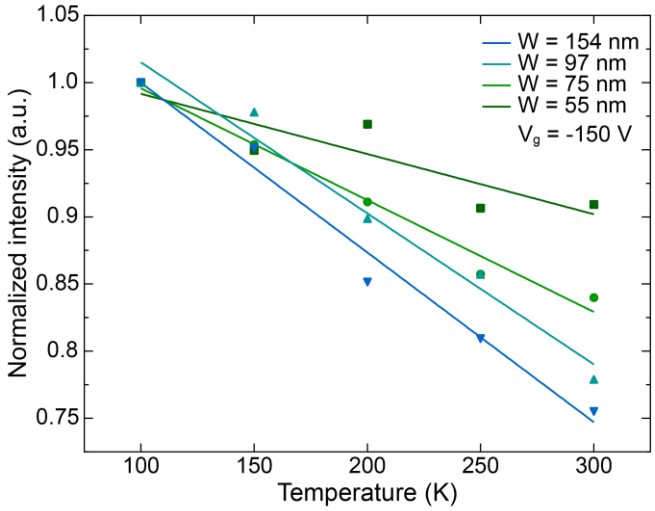

Figure S9. The normalized intensities of the GP extinction peak as a function of temperature at $V_g = -150$ V for various resonator width W (values are in the legend). The symbols represent measured data, and the solid lines are the linear fits. The slopes of each fitted line are -0.05, -0.08, -0.11, and -0.13 %/K for W = 55, 75, 97, and 154 nm, respectively.

References

1. Luk'yanchuk, B.; Zheludev, N. I.; Maier, S. A.; Halas, N. J.; Nordlander, P.; Giessen, H.; Chong, C. T., The Fano resonance in plasmonic nanostructures and metamaterials. *Nat. Mater.* **2010,** *9* (9), 707-715.
2. Falkovsky, L. A.; Varlamov, A. A., Space-time dispersion of graphene conductivity. *Eur. Phys. J. B* **2007,** *56* (4), 281-284.